Vijeth N. Bhat and Vinod L. Gaikwad*

Targeting P-glycoprotein-mediated drug resistance: *in silico* screening and *in vitro* evaluation of phytochemicals

https://doi.org/10.1515/tsd-2025-2709
Received November 6, 2025; accepted December 20, 2025;
published online January 29, 2026

Abstract: Cancer remains one of the significant causes of mortality throughout the globe, with treatment often requiring prolonged therapy. Multidrug resistance, primarily mediated by P-glycoprotein (P-gp) transporters, poses a considerable challenge in the long-term treatment of cancer. To overcome this, P-gp inhibitors can be co-administered for improved drug accumulation and therapeutic efficacy. In the present study, a total of 37 phytochemicals were evaluated for their potential P-gp blocking activity using molecular docking and Molecular Mechanics/Generalized Born Surface Area analysis against the P-gp protein (PDB ID: 6FN1) and compared with Verapamil as a reference P-gp inhibitor. Among the screened compounds, Andrographolide demonstrated the most favourable binding interactions and was further subjected to molecular dynamics simulations, confirming its stable interaction with P-gp. Subsequent *in vitro* cell line studies revealed that Andrographolide, at effective inhibitory concentrations, did not exhibit inherent cytotoxicity but significantly enhanced the cell internalization and cytotoxicity of paclitaxel, a known P-gp substrate. This suggests that Andrographolide plays a role in reversing multidrug resistance through P-gp inhibition, rather than direct cell killing, for effective cancer therapy. These findings indicate that co-administration of phytochemicals, such as Andrographolide, may enhance cell internalization and the efficacy of anticancer drugs, thereby improving chemotherapy outcomes.

Keywords: cancer; phytochemical; P-gp efflux pump inhibitor; multidrug resistance; molecular docking; Caco2 cell-line

***Corresponding author: Vinod L. Gaikwad**, Department of Pharmaceutics, National Institute of Pharmaceutical Education and Research (NIPER), 844 102 Hajipur, Bihar, India,
E-mail: vinod_gaikwad29@yahoo.com
Vijeth N. Bhat, Department of Pharmaceutics, National Institute of Pharmaceutical Education and Research (NIPER), 844 102 Hajipur, Bihar, India

Abbreviations

2D	Two-dimensional
ABC	ATP-binding Cassette
DMEM	Dulbecco's Modified Eagle Medium
DMSO	Dimethyl Sulfoxide
EDTA	Ethylenediaminetetraacetic Acid
EPI	Efflux Pump Inhibitor
FBS	Fetal Bovine Serum
MD	Molecular Dynamics
MDR	Multidrug Resistance
MM-GBSA	Molecular Mechanics/Generalized Born Surface Area
MTT	3-(4,5-Dimethylthiazol-2-yl)-2,5-diphenyltetrazolium Bromide
OPLS	Optimized Potentials for Liquid Simulations
PDB	Protein Data Bank
P-gp	P-glycoprotein
PTX	Paclitaxel
RMSD	Root Mean Square Deviation
SASA	Solvent Accessible Surface Area

1 Introduction

Cancer ranks among the significant causes of mortality, with 1 in 6 deaths reported globally due to a lack of early-stage detection. However, treating cancer became more challenging due to problems associated with chemotherapeutic agents.[1,2] While studying leukaemia in a mouse model, Burchenal et al.[3] reported multidrug resistance (MDR) as one of the major post-diagnosis obstacles in cancer treatment. Furthermore, membrane-bound transporters, such as ATP-binding cassette (ABC) proteins, play a crucial role in MDR, reducing therapeutic efficacy by facilitating the efflux of xenobiotics out of the cell.

The P-glycoprotein (P-gp), a key ABC transporter, is primarily expressed in tumour cells and is responsible for drug efflux and MDR, influencing intracellular drug concentration and targeted chemotherapy.[4,5] The MDR can be overcome by inhibiting the activity of P-gp. The P-gp is a membrane protein, primarily found in organs that eliminate drugs, where it reduces cell burden by mitigating both endogenous and exogenous substrates. The P-gp is located in

phospholipid bilayers and consists of two homologous transmembrane domains and one cytoplasmic nucleotide-binding domain.[6] These membrane proteins are well-known for protecting the cell from death due to high intracellular drug concentrations.[2,7,8]

Delivering multiple drugs with synergistic effects using a single platform is the predominant strategy for effectively managing cancer. P-gp can bind to a wide variety of drug substrates, which leads to drug resistance. Therefore, competitive blocking of P-gp can be achieved by co-administering an inhibitor at a low concentration that has a higher affinity for P-gp than the drug. Moreover, previous studies have demonstrated that the glutamate residue in P-gp is essential for ATPase activity, and any mutations in this residue can significantly impact ATP hydrolysis and P-gp's drug efflux functionality.[9]

The use of phytochemicals as a form of medicine has grown in recent years, and their efficacy in treating or enhancing the action of drugs is well-established. *The in silico* approach has proven to be a promising tool in drug discovery, drug delivery, and regulatory applications.[5,10–14] Scientists worldwide are continually attempting to investigate compounds with P-gp inhibitory potential using computational methods to save time, materials, and costs incurred in experimental trials.[2,8,15]

Andrographolide is a natural phytochemical derived from *Andrographis paniculata,* a plant belonging to the Acanthaceae family. It is widely recognized for its diverse healing benefits, including potent antioxidant activity primarily through free radical scavenging, as well as anti-inflammatory and anticancer effects.[16] Andrographolide is found to modulate multiple proteins and signalling pathways, thereby conferring various protective effects.[17] Moreover, Andrographolide, in combination with certain anticancer drugs, exhibits synergistic cytotoxicity and helps overcome tumour cell resistance to chemotherapy.[18] Studies have reported that Andrographolide inhibits the protein level of CYP3A4, which is directly related to the inhibition of P-gp. It is also noted that compounds inhibiting Cytochrome P450 enzymes are often inhibitors of P-gp.[19,20]

In the present study, 37 phytochemicals with potential P-gp downregulatory activity were selected and evaluated using *in silico* approaches. For molecular docking and interaction studies, the ABCB1 subfamily P-gp membrane protein [protein data bank (PDB) ID: 6FN1] was retrieved from the RCSB PDB.[21] Verapamil, a well-established P-gp inhibitor known to restore drug sensitivity in resistant cancer cells, served as the reference standard.[22] Further, phytochemicals that exhibit promising interactions and binding with the target protein were evaluated using molecular mechanics/generalized born surface area (MM-GBSA) calculations. The compounds demonstrating favourable binding profiles and structural superimposition with the reference standard at the active site were subjected to molecular dynamics (MD) simulations to assess the stability of binding and conformational behaviour. Consequently, the best-performing phytochemical from *in silico* screening was further selected for an *in vitro* cytotoxicity assay using cancer cell lines.

2 Materials and methods

2.1 Materials

Andrographolide (5.46 % assay content in dry herb extract of *Andrographis Paniculata*, batch number: AP/240501) was offered as a free sample by Sunpure Extracts Pvt. Ltd. (U.P., India). Paclitaxel (PTX) was generously supplied by Fresenius Kabi (New Delhi, India). Verapamil Hydrochloride was purchased from Chemicea Pharmaceuticals Pvt. Ltd. (Mumbai, India). Rifampicin was procured from Yarrow Chem Products (Mumbai, India). Dimethyl sulfoxide (DMSO, 99.8 %, for molecular biology), Isopropanol (99 %), and Phosphate buffer saline (10X, Molecular biology grade) were obtained from SRL Pvt. Ltd. (Mumbai, India). For cell culture studies, Dulbecco's Modified Eagle Medium (DMEM, high glucose, 1X), Fetal Bovine Serum (FBS), Trypsin-Ethylenediaminetetraacetic acid (EDTA) (0.5 %, 10X, without phenol red), and Antibiotic-Antimycotic Solution (100X, endotoxin-tested) were procured from Thermo Fisher Scientific (Mumbai, India) and HiMedia Laboratories Pvt. Ltd. (Mumbai, India). MTT (3-(4,5-Dimethylthiazol-2-yl)-2,5-diphenyltetrazolium Bromide, ≥98 % purity) was purchased from SRL Pvt. Ltd. (Mumbai, India). Ultrapure water (Type 1) generated in-house was used throughout the study.

2.2 Software tools and equipment

The chemical structures of ligands and the primary P-gp protein were retrieved from the PubChem and RCSB PDB databases, respectively. Molecular docking, MD simulations, MM-GBSA calculations, and structural superimposition studies were carried out using the Schrödinger Suite (Maestro, version 2025-1). Further, GraphPad Prism software (version 8.0.1) was used to estimate the IC50 (half-maximal inhibitory concentration) value.

Experimental studies were performed using equipment and instruments, including SpectraMax Plus 384 Microplate Reader (Molecular Devices, USA), microbalance (Sartorius, Germany and Aczet Pvt. Ltd., India), UV cabinet (Supertek

Glassware, India), inverted microscope (Zeiss, Germany), cell centrifuge (Eppendorf 5702, Germany), CO_2 incubator (CellXpert, Eppendorf, Germany), clean air cabinet (Baker, Biocompare, USA), and ultrapure (Type 1) water purification system (Milli-Q plus, Millipore, Bedford, USA).

2.3 Methods

2.3.1 *In silico* study

An extensive bibliographic search was performed to build a library of phytochemicals with potential P-gp inhibitory activity, comprising 38 compounds (37 phytochemicals and Verapamil as a reference drug). A preliminary molecular docking study was conducted to evaluate the interaction between the selected compounds and the P-gp transporter protein (PDB ID: 6FN1). The Glide score served as the primary screening criterion, wherein compounds with a Glide score above −6.00 were selected for further analysis. Subsequently, MM-GBSA calculation was performed to determine the binding energy (ΔG_bind) between the two binding partners. A total of 18 promising compounds exhibiting higher binding energy than Verapamil were shortlisted. Subsequently, key amino acid residues involved in binding were identified by analysing the interaction patterns of these shortlisted molecules. Furthermore, superimposition studies were performed by aligning the docked postures with the reference structure (Verapamil) to assess spatial similarity and confirm binding alignment. The most promising compounds were further subjected to MD simulations to evaluate the stability of the protein-ligand complexes over time.

Based on computational evaluation, the top-performing compound, suspected to possess potent P-gp inhibitory activity, was selected for further confirmation by *in vitro* cancer cell line studies.

2.3.1.1 In silico preparation of protein

The structure of the transmembrane protein P-gp, retrieved from the Protein Data Bank (PDB ID: 6FN1), belongs to the human-mouse chimeric ABCB1 subfamily of proteins. The multidrug transporter ABCB1 (P-gp) is an ATP-binding cassette transporter that protects tissues and cells from toxic xenobiotics and expels the drugs outside the cell.[21,23] The protein structure was analysed, revealing the presence of a co-crystallized ligand, Zosuquidar, a well-known P-gp inhibitor used to define sites. These active sites served as a reference for evaluating the interactions of the selected compounds with the P-gp protein. Using a protein preparation wizard in Maestro®, the 6FN1 protein was prepared by adding missing residues or chains, hydrogen atoms, and disulfide bonds, and removing water molecules (except those with strong interactions with the ligand).[24]

2.3.1.2 In silico preparation of ligands

Chemical structures of selected phytochemicals were obtained in 3D SDF file format from the PubChem database. The LigPrep module of the Schrödinger suite was used to optimize the ligand structures after they were imported into the Maestro®. The optimized potentials for liquid simulation (OPLS4) force field was used to minimise energy. The Epik configuration tool was used to prepare all ionization (protonation) and tautomeric forms at a physiological pH (7 ± 2).[25,26]

2.3.1.3 Glide docking

The grid box was created using Maestro®'s receptor grid generation tool. The centre of the box was defined using the co-ordinates of the co-crystalized ligand Zosuquidar (X = 152.84, Y = 150.93, and Z = 148.98), which was already attached to the protein. Moreover, during docking studies, the grid box size was uniformly set to x = 24 Å, y = 24 Å, and z = 24 Å. Van der Waals radii of the receptor atoms were scaled with partial atomic charge less than 0.25 (Cutoff) with a scaling factor of 1, and non-polar parts of the ligand with 0.15 (cutoff) with a scaling factor of 0.80. The co-crystalized ligand was removed during grid preparation to enable the ligand of interest. Glide docking was then performed to evaluate the glide score and analyse the interaction of the ligand within the active site.[27]

2.3.1.4 Prime MM-GBSA calculations

The best glide poses obtained from glide docking were selected to estimate the binding free energy (ΔG_bind) of ligands with 6FN1, using the MM-GBSA method. The variable Dielectric Generalized Born Solvation Model was employed to calculate solvation free energy in the context of protein-ligand binding. MM-GBSA provides a more realistic estimation of binding affinity under near-physiological conditions than the static docking state. While the glide score is the primary criterion for initial ligand ranking, MM-GBSA acts as supportive data to refine and validate binding interactions. Unlike glide docking, which does not account for solvent or entropy effects, MM-GBSA incorporates solvent effects through an implicit solvent model, thereby providing a more reliable prediction of binding energy.[28]

2.3.1.5 Superimposition estimation

Superimposition involves aligning docked ligand poses to a reference structure, often based on overall shape or a common scaffold, to facilitate structural comparisons and

analysis. This process helps to assess how closely a docked pose matches a reference pose. A standard metric used for this purpose is the root mean square deviation (RMSD), where a lower RMSD value indicates a closer alignment and better agreement between the two poses. In the present study, ligand entries from the workspace were superimposed with Verapamil as a reference structure. The docked ligand poses were aligned without altering their structural conformations. The maximum common substructure between each ligand and Verapamil was identified, and superimposition was performed using atom specification language. The degree of alignment with the reference compound was then assessed by calculating the RMSD.[29,30]

2.3.1.6 Molecular dynamics simulation

The docked ligand-protein complex was used to build a simulation system comprising protein, ligand, solvent (TIP3P model), salts and ions. An orthorhombic box was created with a distance of 10 Å from the complex, and the OPLS4 force field was applied. The system was neutralized by adding counter-ions, primarily sodium and chloride ions, which were automatically calculated in Maestro®, and physiological salt conditions were maintained. A production MD simulation was performed for 100 ns, with trajectory frames recorded every 100 ps. The temperature and pressure were maintained at 300 K and 1.01325 bar, respectively. The system was relaxed using standard equilibration protocols before the run. Post-simulation data were analysed to calculate the RMSD, protein-ligand contacts and ligand properties during simulation, to evaluate the stability of the structure and the flexibility of the complex.[31,32]

2.3.2 *In vitro* cell line studies

The Caco-2 pure cell strain was revived and cultured in DMEM supplemented with 10 % FBS and 1 % antibiotic-antimycotic solution. The cells were kept at 37 °C with 5 % CO_2 in a humidified incubator. For subculturing, cells were detached using 1X trypsin-EDTA solution. For cell lysis during experiments, a 0.1 % Triton X-100 solution was used.[33]

2.3.2.1 Cytotoxicity assay

The cytotoxicity of Andrographolide was evaluated using the MTT assay, which measures the reduction of yellow MTT to purple formazan crystals by mitochondrial succinate dehydrogenase enzyme in viable cells. 10 thousand cells per well were seeded in a 96-well plate and incubated for 24 h at 37 °C to allow for attachment. The medium was then replaced with fresh medium containing various concentrations of PTX (12.5–200 µg mL^{-1}). After 24 h of treatment, 100 µL of 0.5 mg mL^{-1} MTT was added, and the plates were incubated in the dark for 3 h. The medium was removed, and the formed formazan crystals were dissolved in 100 µL DMSO using a shaker for 30 min. Furthermore, absorbance was measured at 570 nm using a SpectraMax Plus 384 Microplate Reader. Experiments were performed in triplicate, and IC_{50} values were calculated.[34,35]

2.3.2.2 Assessment of efflux pump inhibition

The effect of efflux pump inhibitor (EPI) on PTX (a P-gp substrate) internalization was evaluated using six treatment groups: I) Normal Control, II) PTX (100 µg mL^{-1}), III) PTX + Verapamil (200 µg mL^{-1}), IV) PTX + Verapamil (100 µg mL^{-1}), V) PTX + Andrographolide (200 µg mL^{-1}), and VI) PTX + Andrographolide (100 µg mL^{-1}). 10 thousand cells per well were seeded in a 96-well plate and incubated at 37 °C for 24 h to allow for attachment. P-gp expression was induced by treating cells with 20 µM rifampicin for 24 h. After medium removal, fresh medium containing respective EPI concentrations was added, followed by the standard MTT assay to assess P-gp inhibition and cell viability.[36]

3 Result and discussion

3.1 *In silico* study: glide docking

The chemical structures of 37 phytochemicals, identified through bibliographic research, along with that of Verapamil (reference compound), are presented in Figure 1a and Figure 1b. Verapamil is established as a first-generation P-gp inhibitor. Among other tested compounds, such as Zosuquidar and Elacridar (which have not been approved), Verapamil stands out due to its proven clinical use with a well-known mechanism of action. Therefore, in the present study, Verapamil was used as a reference compound for screening proposed phytochemicals as P-gp inhibitors, due to its ease of availability, established safety profile and P-gp inhibitory activity.[37,38] All these ligands were docked with the P-gp protein (PDB ID: 6FN1) to estimate their Glide scores and assess their binding affinities. Glide score is a computational estimate of the binding affinity between two binding partners, incorporating various interaction parameters such as Van der Waals forces, electrostatic interactions, hydrogen bonding, and hydrophobic effects.[39] A more negative glide score indicates more stable and spontaneous interactions with the active site residues. Accordingly, six phytochemicals demonstrated better glide scores than Verapamil (−8.011, Table 1).[40]

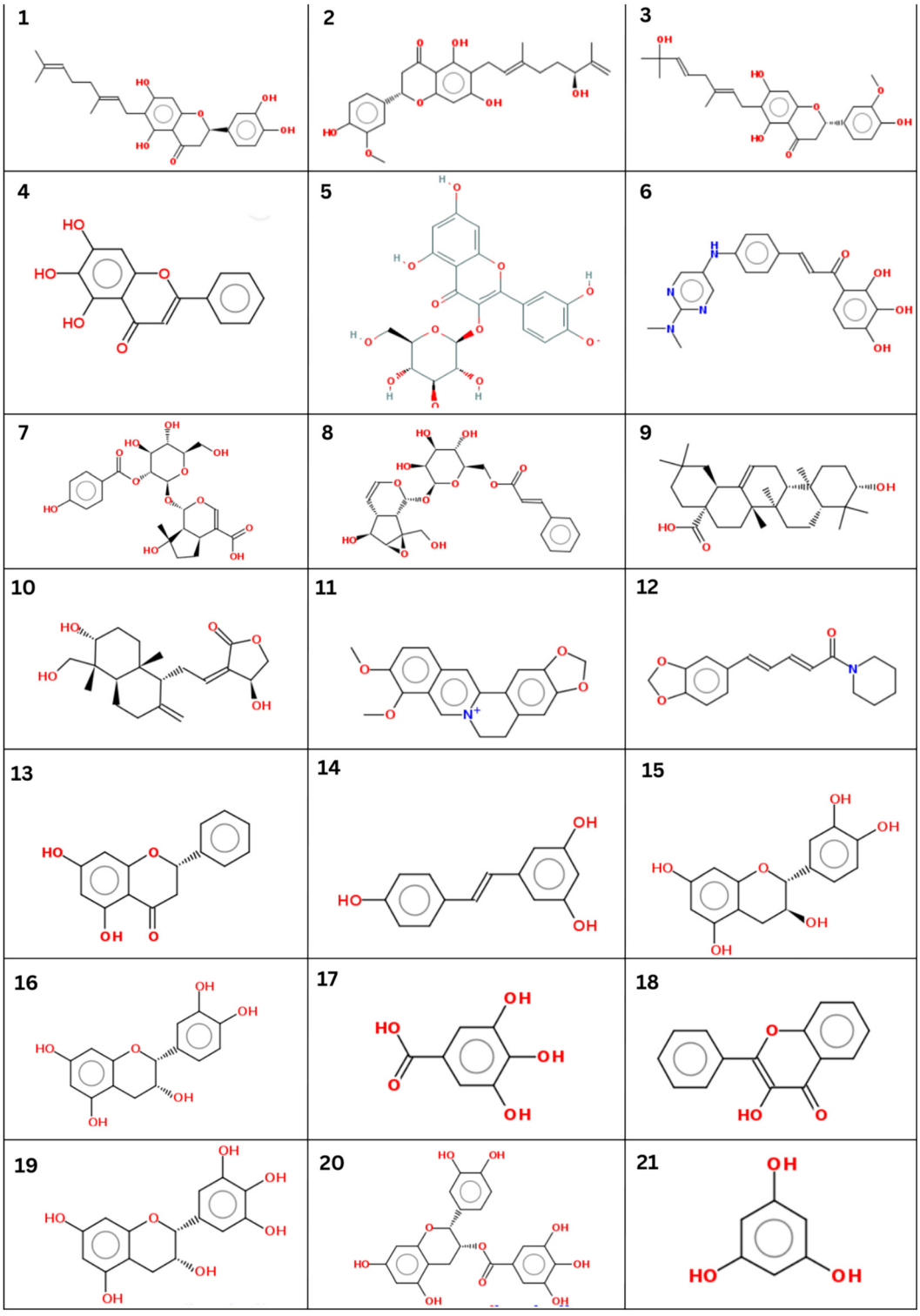

(a)

Figure 1a: Chemical structures of ligands: (1) Diplacone, (2) Tomentodiplacone M, (3) Tomentodiplacone B, (4) Baicalein, (5) Quercetin-3-glucoside, (6) Chalcones, (7) Negundoside, (8) Picroside-I, (9) Oleanolic acid, (10) Andrographolide, (11) Berberine, (12) Piperine, (13) Pinocembrin, (14) Resveratrol, (15) Catechin, (16) Epicatechin, (17) Gallic acid, (18) 3-Hydroxyflavone, (19) Epigallocatechin, (20) Epicatechin gallate, and (21) Phloroglucinol.

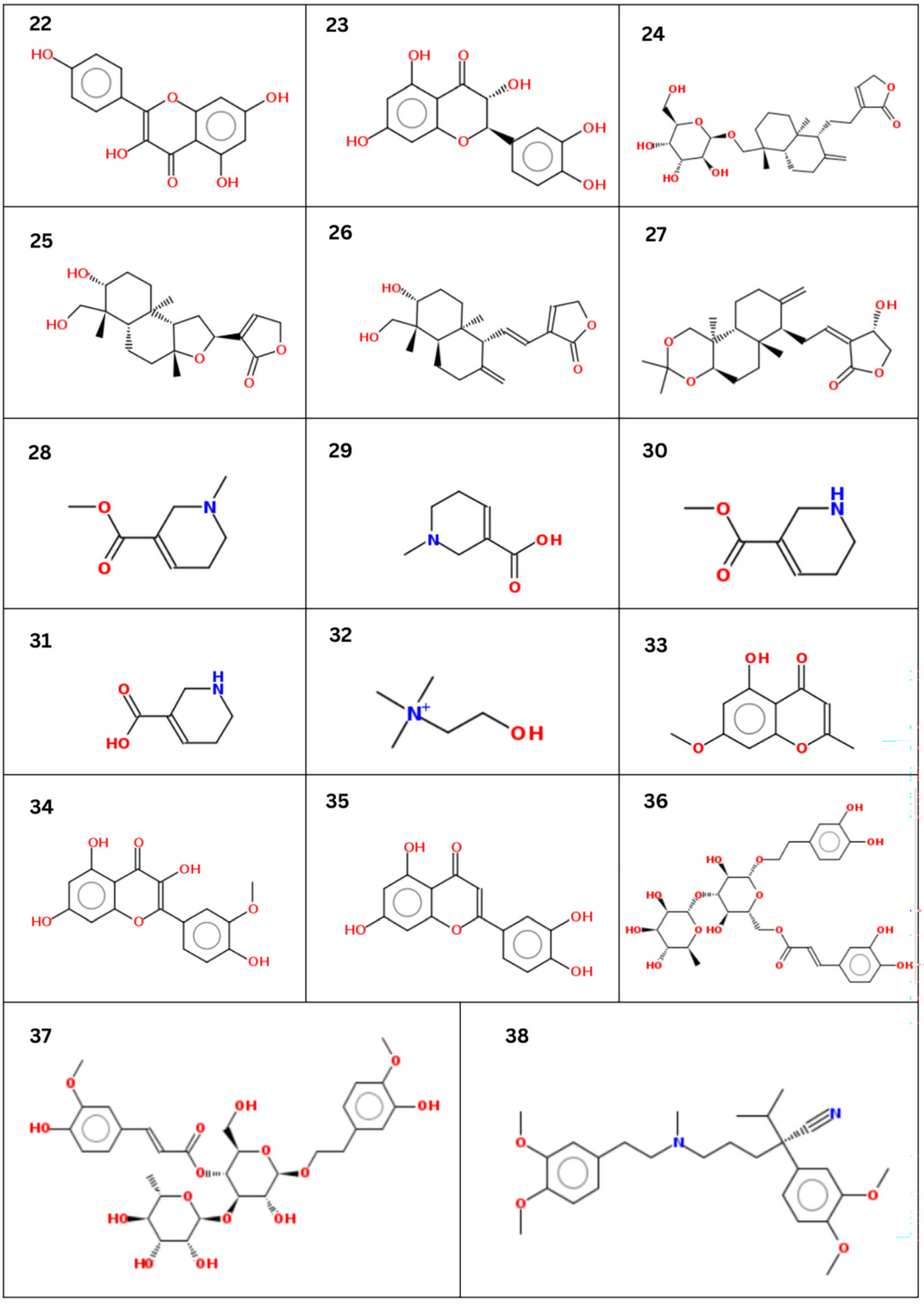

(b)

Figure 1b: Chemical structures of ligands: (22) Kaempferol, (23) Taxifolin, (24) Neoandrographolide, (25) Isoandrographolide, (26) 14-deoxy-11,12-didehydroandrographolide, (27) 3,19-isopropylidene andrographolide, (28) Arecoline, (29) Arecaidine, (30) Guvacoline, (31) Guvacine, (32) Choline, (33) Eugenin, (34) Isorhamnetin, (35) Luteolin, (36) Isoacteoside, (37) Martynoside, and (38) Verapamil.

Table 1: Glide scores of selected compounds against P-gp (PDB ID: 6FN1).

Sl. No.	Compound	Glide score	Sl. No.	Compound	Glide score
1.	Verapamil	−8.011	20.	Pinocembrin	−7.053
2.	Martynoside	−8.519	21.	Baicalein	−6.806
3.	Tomentodiplacone B	−8.41	22.	Picroside-I	−6.639
4.	Tomentodiplacone M	−8.302	23.	Andrographolide	−6.471
5.	Epicatechin gallate	−8.148	24.	Iso-andrographolide	−6.426
6.	Isorhamnetin	−8.023	25.	Phloroglucinol	−6.403
7.	Isoacteoside	−8.552	26.	Eugenin	−6.342
8.	Piperine	−7.883	27.	Guvacoline	−6.248
9.	Resveratrol	−7.868	28.	14-deoxy-11,12-didehydroandrographolide	−6.248
10.	Negundoside	−7.716	29.	3,19-isopropylideneandrographolide	−6.18
11.	Kaempferol	−7.708	30.	3-Hydroxyflavone	−6.012
12.	Epicatechin	−7.652	31.	Gallic acid	−5.698
13.	Diplacone	−7.584	32.	Quercetin-3-glucoside	−5.642
14.	Epigallocatechin	−7.52	33.	Neoandro-grapholide	−5.454
15.	Berberine	−7.424	34.	Arecoline	−5.348
16.	Chalcones	−7.394	35.	Arecaidine	−5.337
17.	Catechin	−7.34	36.	Guvacine,	−5.281
18.	Taxifolin	−7.297	37.	Oleanolic acid	−5.278
19.	Luteolin	−7.085	38.	Choline	−4.294

Subsequently, 30 phytochemicals showing a glide score above the threshold (−6.00) were selected for MM-GBSA studies to estimate binding free energy more accurately. The threshold value of −6.00 was set to include the maximum number of compounds.

3.2 Prime MM-GBSA calculations

Glide score is a scoring function used in molecular docking to evaluate various non-covalent interactions between two binding partners. In contrast, MM-GBSA provides a more detailed insight into protein-ligand interactions by calculating the complete binding free energy (Table 2). This method accounts for multiple contributions to binding energy, including electrostatic interactions and solvent effects.[41,42]

Ligand and protein binding are dependent on the laws of thermodynamics. The Gibbs binding free energy is expressed by Equation (1).[43]

$$\Delta G = \Delta H - T\,\Delta S \quad (1)$$

Where ΔG is the change in Gibbs free energy, ΔH is the change in enthalpy (heat absorbed or released), ΔS is the

Table 2: Binding free energy (ΔG_bind) values calculated by MM-GBSA for selected compounds against P-gp.

Sl. No.	Compound	MM-GBSA (kcal mol^{-1})	Sl. No.	Compound	MM-GBSA (kcal mol^{-1})
1.	Verapamil	−77.17	16.	Epicatechin gallate	−112.41
2.	Martynoside	−122.1	17.	Catechin	−115.4
3.	Tomentodiplacone B	−94.4	18.	Taxifolin	−195.3
4.	Tomentodiplacone M	−59.97	19.	Luteolin	5.38
5.	Isorhamnetin	−37.13	20.	Pinocembrin	101.37
6.	Isoacteoside	−134.97	21.	Baicalein	−82.49
7.	Piperine	4.4	22.	Picroside-I	−110.07
8.	Resveratrol	27.75	23.	Andrographolide	−105.51
9.	Negundoside	−52.33	24.	Iso-andrographolide	−28
10.	Kaempferol	−115.54	25.	Phloroglucinol	−28.98
11.	Epicatechin	−95.91	26.	Eugenin	−112.72
12.	Diplacone	−8.38	27.	Guvacoline	100.84
13.	Epigallocatechin	−9.35	28.	14-deoxy-11,12-didehydroandrographolide	−158.18
14.	Berberine	−120	29.	3,19-isopropylideneandrographolide	−36.95
15.	Chalcones	−100.91	30.	3-Hydroxyflavone	−8.33

change in entropy (disorder or randomness) of the system upon the binding of the ligand, and T is the absolute temperature in Kelvin.

The reaction is random and spontaneous when ΔG is negative, whereas a positive ΔG indicates a non-spontaneous process. The ΔG, representing the overall change in free energy, encompasses both enthalpic and entropic contributions that occur during the binding of two interacting partners, typically a protein and a ligand.

The reference compound, Verapamil, exhibited a ΔG value of $-77.17\,\text{kcal mol}^{-1}$, while 14-deoxy-11,12-didehydroandrographolide showed the highest spontaneity against the P-gp active site with a ΔG value of $-158.18\,\text{kcal mol}^{-1}$ (Table 2). A more negative ΔG_bind compared to Verapamil suggests that the selected phytochemical-protein complexes are more stable and potentially possess greater inhibitory activity against P-gp than the reference compound.[44] Therefore, 18 phytochemicals demonstrating a higher binding free energy (either a negative or a positive value) than the reference ($-77.17\,\text{kcal mol}^{-1}$) were selected for the screening study.

These 18 phytochemicals were critically analysed based on their interaction diagrams, the amino acids involved in binding, and the similarity in overlapping with Verapamil's interaction at the P-gp active site. It has been observed that Verapamil, along with Tomentodiplacone B, Tomentodiplacone M, Epicatechin gallate, Andrographolide, and 14-deoxy-11,12-didehydroandrographolide, share 19, 16, 17, 15, and 16 common amino acid interactions, respectively, within the active site.

A high similarity with the reference compound suggests that these phytochemicals may mimic Verapamil's activity. Table 3 summarises common amino acids shared with the reference (highlighted with underline), and hydrogen bonds formed between amino acid residues of P-gp and ligands (highlighted in bold). Generally, a greater number of hydrogen bonds corresponds to more stable interactions, which facilitates a more spontaneous binding process.[45,46] The two-dimensional (2D) diagrams of these interactions are presented in Figure 2a and Figure 2b.

3.3 Superimposition estimation

The docked pose of Verapamil was superimposed with that of phytochemicals, and the extent of alignment was evaluated using the RMSD value (Table 4). Andrographolide and 14-deoxy-11,12-didehydroandrographolide exhibited the least structural deviation, aligning best with the Verapamil docking pose (Figure 3), with RMSD values of 5.8134 Å and 5.960, respectively (Table 4). This suggests possible reproducibility of the experimental binding modes similar to that of the reference compound.[47]

Andrographolide, in particular, showed the closest alignment with the standard drug pose and performed best overall, demonstrating a favourable glide score of −6.471 and a Gibbs binding free energy of $-105.51\,\text{kcal mol}^{-1}$, indicative of the total system energy. This includes real-time interactions, solvent effects and entropy contributions, supporting its potential as an effective P-gp inhibitor. [48]

3.4 Molecular dynamics simulation

Verapamil and Andrographolide were subjected to 100 ns of MD simulations separately with the 6FN1 protein to assess the ligand's binding stability with the active sites of P-gp. The *in vivo* environment was created by surrounding the protein-ligand complex with solvent molecules neutralized by ions and salts, to assess the stability of the complex in a physiological environment. Further, the MD simulation report was evaluated for protein-ligand RMSD, protein-ligand contacts, and ligand properties.

The Verapamil persistently stayed within the active site, as evidenced by Verapamil's confirmations and orientations captured at different time points during the simulation study (Figure 4). This indicates the stability of the interactions between Verapamil and the P-gp (6FN1 protein).

Figure 5A shows the stability of the Verapamil-P-gp complex during the course of the 100-nanoseconds simulation study. The conformational changes observed within the defined study time frame are minimal, with the protein RMSD (blue line in Figure 5A) ranging from 2.5 to 5 Å. In contrast, the ligand RMSD (red line in Figure 5A) varied between 3 and 4.2 Å, indicating excellent stability of the complex. This suggests the Verapamil-P-gp complex retained its structural integrity without experiencing notable conformational changes during the simulation study.[49] The change in the RMSD value of protein and ligand indicates the mobility of the protein and ligand over time, wherein a high value of RMSD is related to high mobility and vice versa. [50]

Figure 5B and C illustrate the stability of Verapamil-protein residue contacts, reflecting the strength of interactions between Verapamil and amino acid residues. The residues PHE302, TYR306, PHE335, PHE769, and PHE982 exhibited robust and stable interactions over a period of 100 ns, while TRP231, GLN772, and GLN837 showed intermediate stability in their interactions with Verapamil. Notably, TYR306, GLN724, GLN772 and GLN837 are significantly involved in forming direct or water-bridge hydrogen bonds contributing to the enhanced stability of the binding partners. These non-covalent bonds and their stability

Table 3: Amino acid residues of P-gp involved in interactions with selected ligands.

Sl. No.	Compound	Amino acid residues involved in the interaction
1.	Verapamil	MET98, ASN295, MET298, PHE302, ILE305, **TYR306**, TYR309, ASN720, GLY721, LEU723, **GLN724,** PHE727, **SER765,** PHE769, GLN772, GLN837, ASN841, TYR952, PHE982, MET985, ALA986, GLN989, VAL990, PHE993.
2.	Isoacteoside	TRP231, LEU235, MET298, **ASN295**, PHE302, **TYR306**, PHE342, GLN720, LEU723, **GLN724**, GLN772, GLY773, SER830, ALA833, GLN837, **GLU874**, MET875, LEU878, ALA986, GLN989, VAL990, PHE993, ALA994, PRO995.
3.	Martynoside	MET68, **TRP231,** LEU235, MET298, PHE302, TYR309, PHE335, GLN346, ASN720, PHE769, GLN772, GLN837, **GLU874**, MET875, LEU878, TYR952, PHE982, MET985, ALA986, **GLN989,** VAL990, PHE993.
4.	Tomentodiplacone B	ASN295, MET298, PHE302, ILE305, TYR306, **TYR309, ASN720,** LEU723, GLN724, PHE727, SER765, PHE769, GLN772, GLY773, SER830, ALA833, VAL834, GLN837, PHE982, ALA986, GLN989, VAL990, PHE993, ALA994.
5.	Tomentodiplacone M	TRP231, ASN295, MET298, PHE302, ILE305, TYR306, **TYR309**, LEU338, **GLN724**, PHE727, PHE769, GLN772, GLY773, SER830, ALA833, VAL834, GLN837, PHE982, ALA986, GLN989, VAL990, PHE993, ALA994.
6.	Kaempferol	TRP231, MET298, PHE302, ASN720, LEU723, **GLN724**, PHE769, **GLN772**, GLN837, ALA986, GLN989, VAL990, PHE993, ALA994.
7.	Epicatechin	ASN295, MET298, PHE302, TYR306, ASN720, LEU723, **GLN724**, PHE769, GLN772, GLY773, **GLN837,** ALA986, GLN989, VAL990, PHE993.
8.	Berberine	MET298, TYR306, ASN720, LEU723, GLN724, PHE769, GLN772, GLN837, PHE982, MET985, ALA986, **GLN989**, VAL990, PHE993.
9.	Chalcones	TRP231, LEU235, **ASN295**, MET298, PHE302, ILE305, PHE342, ASN720, PHE769, GLN772, GLY773, ALA833, GLN837, MET875, GLN989, VAL990, PHE993, ALA994.
10.	Epicatechin gallate	TRP231, ASN295, MET298, PHE302, TYR306, ASN720, GLY721, LEU723, GLN724, SER765, PHE769, GLN772, GLY773, SER830, ALA833, VAL834, **GLN837,** ASN841, MET875, ALA986, GLN989, VAL990, PHE993, ALA994, PRO995.
11.	Catechin	TRP231, **ASN295**, MET298, PHE302, ASN720, PHE769, GLN772, GLY773, PHE776, GLN837, ALA833, MET875, GLN989, VAL990, PHE993, ALA994.
12.	Taxifolin	TRP231, LEU235, **ASN295**, MET298, PHE302, ASN720, PHE769, GLN772, GLY773, PHE776, ALA833, VAL834, GLN837, MET875, GLN989, VAL990, PHE993, ALA994.
13.	Pinocembrin	**ASN295,** MET298, PHE302, PHE769, GLN772, GLY773, SER830, ALA833, VAL834, GLN837, GLN989, VAL990, PHE993, ALA994.
14.	Baicalein	**ASN295,** MET298, PHE302, PHE769, GLN772, GLY773, PHE776, SER830, ALA833, VAL834, GLN837, GLN989, VAL990, PHE993, ALA994.
15.	Picroside-I	**ASN295**, MET298, PHE302, PHE769, GLN772, GLY773, PHE776, SER830, ALA833, VAL834, GLN837, GLN989, VAL990, PHE993, ALA994.
16.	Andrographolide	PHE302, ILE305, TYR306, **ASN720,** GLY721, LEU723, GLN724, PHE727, PHE769, GLN837, ASN841, PHE982, MET985, ALA986, **GLN989,** VAL990.
17.	Eugenin	TRP231, MET298, PHE302, TYR306, **ASN720,** LEU723, GLN724, SER765, PHE769, GLN837, MET875, GLN989, VAL990, PHE993.

Table 3: (continued)

Sl. No.	Compound	Amino acid residues involved in the interaction
18.	Guvacoline	ASN295, MET298, PHE302, **ASN720**, LEU723, PHE769, GLN772, **GLN837**, VAL990, PHE993.
19.	14-deoxy-11,12-didehydroandrographolide	PHE302, ILE305, TYR306, TYR309, **ASN720**, GLY721, LEU723, **GLN724**, PHE727, SER765, PHE769, GLN837, PHE982, MET985, ALA986, GLN989, VAL990.

throughout the simulation period confirm the reaction spontaneity and stability.[51] Figure 5D depicts Verapamil's behaviour during simulation. The radius of gyration (Rg), which estimates the compactness and spatial distribution of the ligand's atoms around its centre of mass, remained approximately 5.9 Å, indicating that Verapamil maintained a stable and compact shape throughout the simulation.[52] The solvent accessible surface area (SASA) observed around 45 $Å^2$ indicates minimal solvent exposure and that the ligand is almost completely buried within the binding pocket. These values also reflect the dynamic folding behaviour of the P-gp protein, further supporting the stability of the structure and moderate accessibility of the ligand during the simulation.[53]

Furthermore, no internal hydrogen bonding within the ligand was detected, indicating that external contacts with the protein govern all interactions. This ensures complete availability of Verapamil for interaction within the active site, potentially enhancing its binding efficiency.

Similarly, the stability of the interaction between Andrographolide and the P-gp was assessed by performing MD simulation for 100 ns. Figure 6 depicts the confirmations and orientations of Andrographolide throughout the simulation period, demonstrating that Andrographolide consistently remained within the protein's active site.

Furthermore, the MD simulation data of Andrographolide with P-gp showed a more stable interaction than the reference (Verapamil). The RMSD of protein was observed in the range of 2.25–4.8 Å (blue line in Figure 7A), while for ligand, the RMSD was recorded between 1.75 and 3.6 Å (red line in Figure 7A). The low RMSD observed for the Andrographolide-P-gp complex indicates its excellent stability compared to the Verapamil-P-gp complex (RMSD between 3 and 4.2 Å, Figure 5A).[32,54] Upon substrate binding, P-gp flips outward, resulting in significant conformational changes and alterations in protein folding, as illustrated by the increased RMSD in simulation analysis. The stable conformation of P-gp when bound to Andrographolide provides evidence of the compound's inhibitory effects on the efflux pump, as well as demonstrating a strong binding efficacy.[55]

The protein-ligand contact plot (Figure 7B) demonstrates the formation of hydrogen bonds, hydrophobic interactions, ionic bonds and other non-covalent interactions between the ligand and amino acid residues in the active site. Moreover, the amino acid residues, namely TYR309, TYR306, ASN720, GLN724, SER765, GLN772, GLN837, ASN841, and GLN989, were found to be involved in hydrogen binding, either directly or through water bridges, contributing significantly to the stability of the Andrographolide-P-gp complex. Usually, a high number of hydrogen bonds correlates with increased interaction stability and spontaneity. Andrographolide exhibits a higher potential for binding efficiently with the active site compared to Verapamil, as evidenced by its capability to form a greater number of hydrogen bonds with the active site residues. This observation is supported by the principles established in thermodynamics, which dictate that the formation of multiple hydrogen bonds can enhance molecular interactions and binding affinity (Equation (1)). Moreover, PHE302, TYR309, ASN720, GLN837, ASN841 and GLN989 residues exhibited stable interactions during the 100-nanosecond simulation period (Figure 7C). The ligand properties recorded during the simulation study (Figure 7D) demonstrated a lower radius of gyration for Andrographolide (around 4.05 Å) compared to Verapamil. This lower radius of gyration indicates a more compact structure, potentially due to the formation of internal hydrogen bonds.[52] Moreover, the SASA recorded for Andrographolide (less than 20 $Å^2$) was significantly lower than the reference, indicating minimal solvent exposure to andrographolide molecules. This demonstrates minimal interaction of ligand molecules with surrounding solvent molecules, suggesting that the ligand is deeply buried within the active site. Such a burial reflects a highly folded protein conformation, confining interactions predominantly to the binding site residues.

These findings demonstrate more stable and effective interactions of Andrographolide with the P-gp active site, potentially contributing to effective P-gp inhibition. Conversely, Verapamil is a well-established synthetic reference EPI, whereas Andrographolide requires further optimization to enhance its efficacy.

3.5 Cytotoxicity assay

The MTT assay of Andrographolide was performed at different concentrations (1–250 μg mL^{-1}) on Caco-2 cells. The

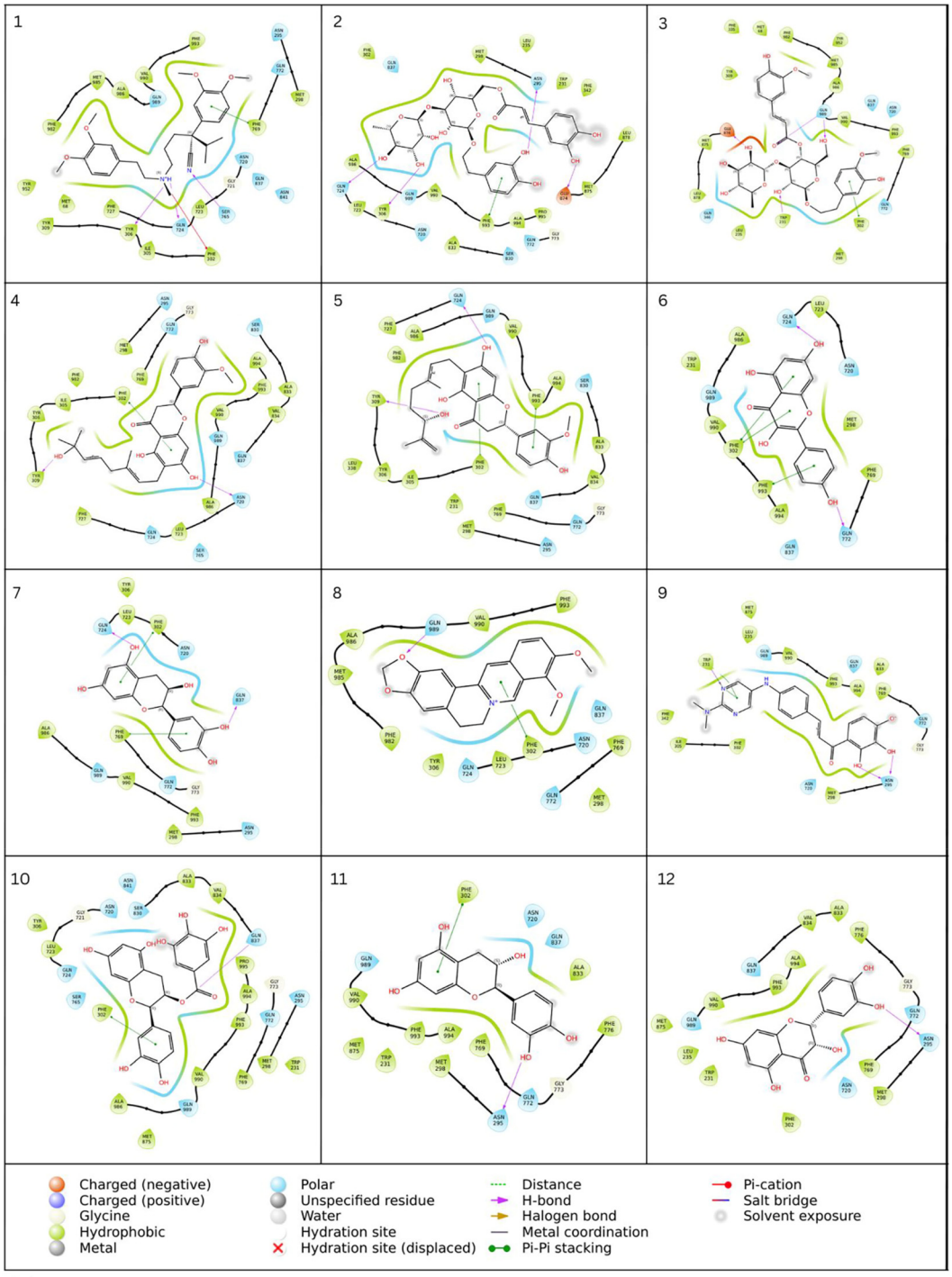

(a)

Figure 2a: Molecular docking interactions between selected compounds and P-gp. 1. Verapamil, 2. Isoacteoside, 3. Martynoside, 4. Tomentodiplacone B, 5. Tomentodiplacone M, 6. Kaempferol, 7. Epicatechin, 8. Berberine, 9. Chalcones, 10. Epicatechin gallate, 11. Catechin, 12. Taxifolin.

results were analysed using a nonlinear regression model using GraphPad Prism (version 8.0.1). The IC_{50} and R^2 values were observed to be 219.7 µg mL^{-1} and 0.8835, respectively. It is clearly evident from the dose-response curve (Figure 8) that Andrographolide is not cytotoxic at low concentrations. Subsequent cellular studies were designed, below the IC_{50} threshold, to evaluate Andrographolide's role as a P-gp inhibitor in combination with PTX (a known P-gp substrate). Moreover, a comparative evaluation with Verapamil (a reference P-gp inhibitor) was also performed to determine

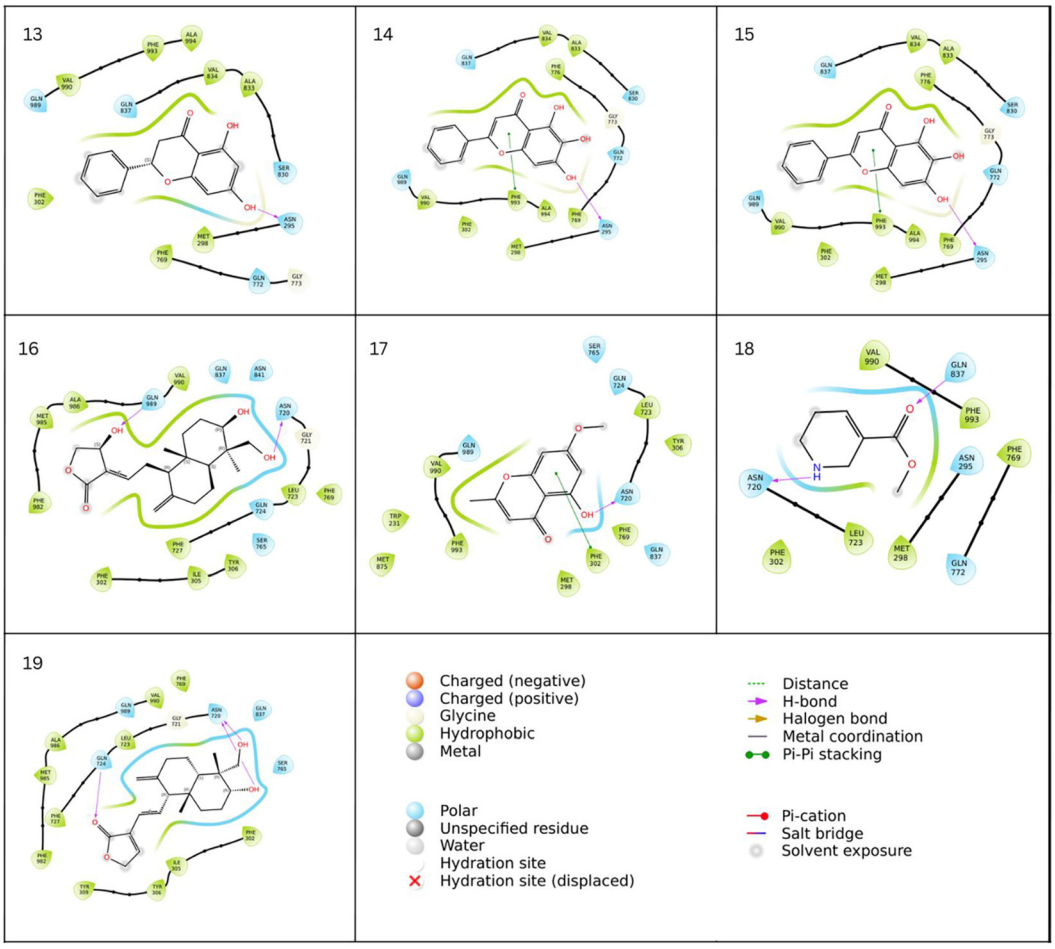

(b)

Figure 2b: Molecular docking interactions between selected phytochemicals and P-gp. 13. Pinocembrin, 14. Baicalein, 15. Picroside-I, 16. Andrographolide, 17. Eugenin, 18. Guvacoline, 19. 14-deoxy-11,12-didehydroandrographolide.

Table 4: RMSD values for the superimposition of docked ligand poses with Verapamil.

Sl. No.	Compound	RMSD (Å) from superimposition	Sl. No.	Compound	RMSD (Å) from superimposition
1.	Verapamil	0	10.	Catechin	8.8908
2.	Isoacteoside	10.0135	11.	Taxifolin	9.7877
3.	Martynoside	10.3253	12.	Pinocembrin	9.9601
4.	Tomentodiplacone B	8.4234	13.	Baicalein	10.6152
5.	Tomentodiplacone M	8.9767	14.	Picroside-I	7.1297
6.	Kaempferol	7.4973	15.	Andrographolide	5.8134
7.	Epicatechin	7.1043	16.	Eugenin	7.2054
8.	Berberine	7.6145	17.	Guvacoline	6.1719
9.	Chalcones	10.1414	18.	14-deoxy-11,12-didehydroandrographolide	5.960
10.	Epicatechin gallate	8.6726			

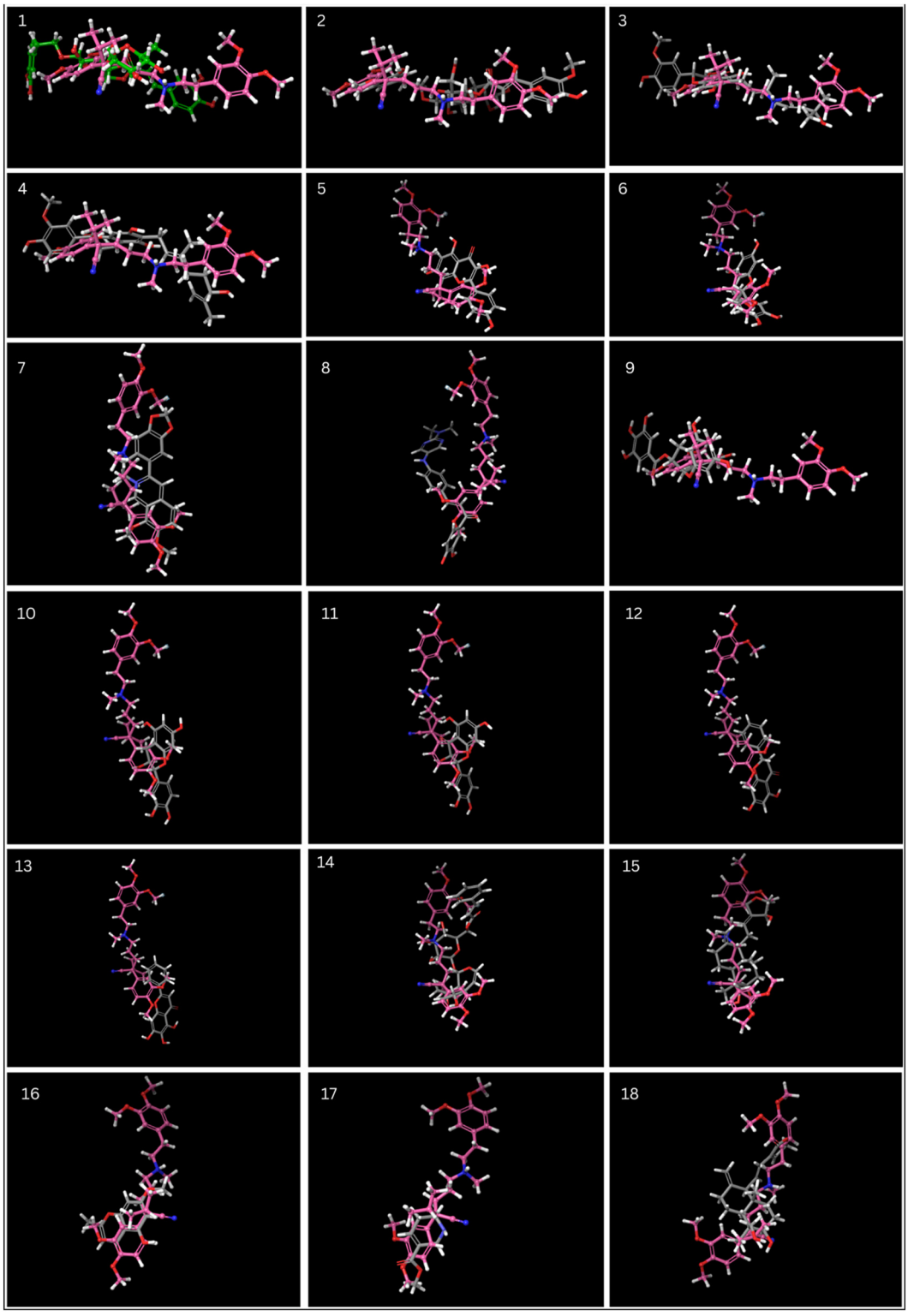

Figure 3: The 2D superimposition of docked ligand poses with the Verapamil (pink). 1. Isoacteoside, 2. Martynoside, 3. Tomentodiplacone B, 4. Tomentodiplacone M, 5. Kaempferol, 6. Epicatechin, 7. Berberine, 8. Chalcones, 9. Epicatechin gallate, 10. Catechin, 11. Taxifolin, 12. Pinocembrin, 13. Baicalein, 14. Picroside-I, 15. Andrographolide, 16. Eugenin, 17. Guvacoline, 18. 14-deoxy-11,12-didehydroandrographolide.

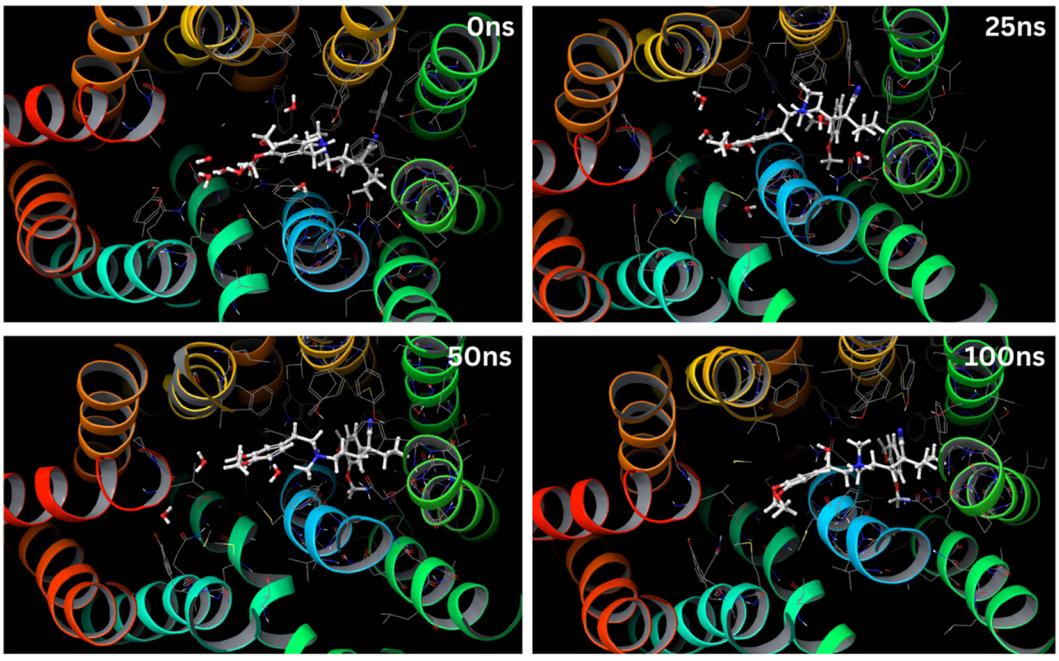

Figure 4: Pictorial presentation of MD simulation depicting the binding conformation of Verapamil within the P-gp protein (6FN1) at different time points.

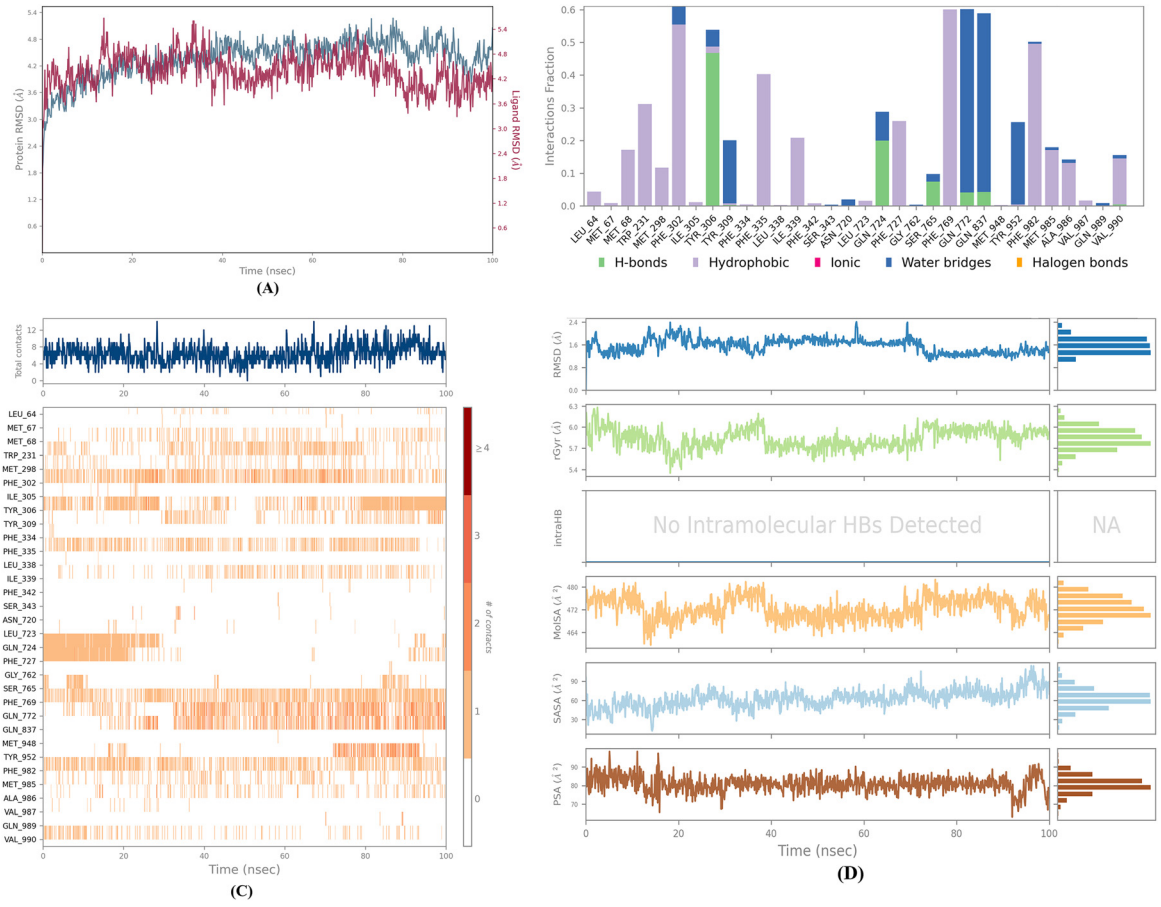

Figure 5: MD simulation data for Verapamil-P-gp (6FN1) complex. (A) Protein-ligand RMSD plot, (B) protein-ligand contacts plot, (C) stability of protein ligand contacts, (D) MD ligand Properties.

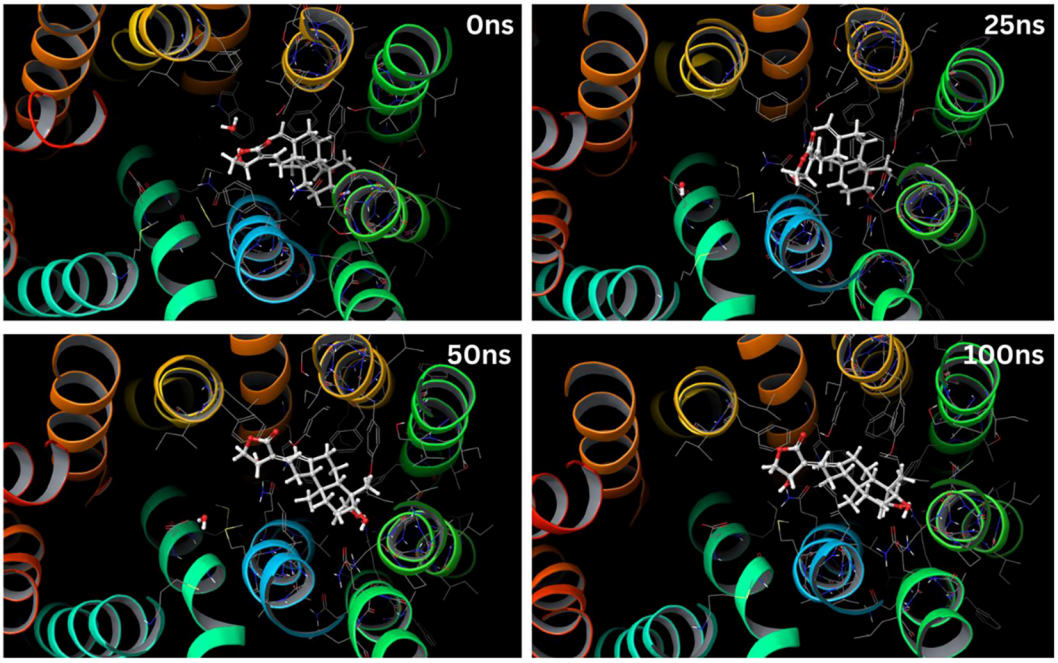

Figure 6: Pictorial presentation of MD simulation depicting the binding conformation of Andrographolide within the P-gp protein (6FN1) at different time points.

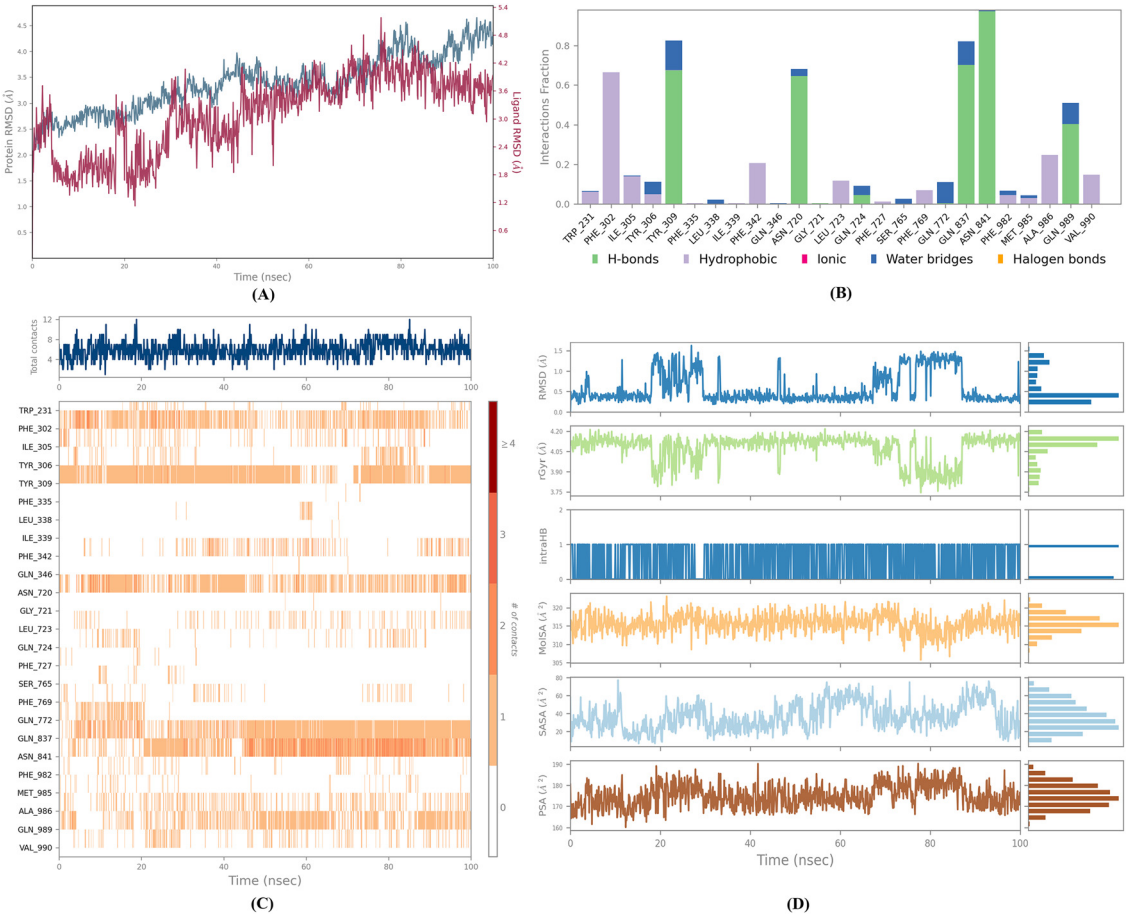

Figure 7: MD simulation data for Andrographolide-P-gp (6FN1) complex. (A) Protein-ligand RMSD plot, (B) protein-ligand contacts plot, (C) stability of protein ligand contacts, (D) MD ligand Properties.

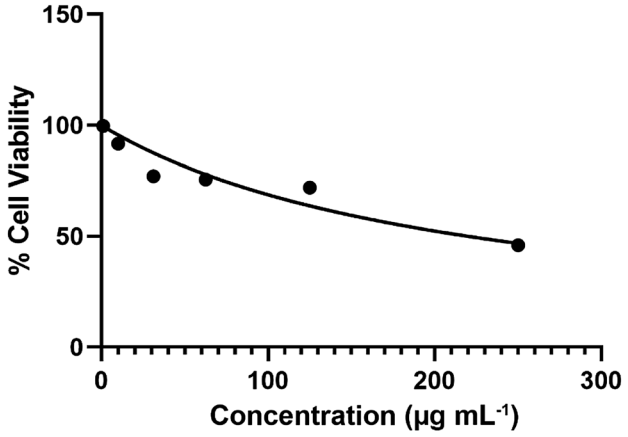

Figure 8: Dose-response curve (MTT assay) of Andrographolide.

the potential of Andrographolide in enhancing the anticancer efficacy by reversing MDR.

3.6 Assessment of efflux pump inhibition

The MTT assay was performed across various treatment groups expressing P-gp using Rifampicin, to evaluate the potential of EPIs (Verapamil and Andrographolide) in enhancing the cell internalization and therapeutic efficacy of PTX.[56]

The cell viability for PTX alone (100 µg mL^{-1}) was 16.00 %. However, when PTX (100 µg mL^{-1}) was combined with Verapamil (100 µg mL^{-1} and 200 µg mL^{-1}), the viability was reduced to 8.53 % and 8.04 %, respectively. These nearly identical values suggest that increasing Verapamil concentration did not induce cytotoxicity alone. Instead, it implies that Verapamil likely improves PTX intracellular accumulation by inhibiting P-gp efflux pump activity, leading to enhanced PTX-mediated cytotoxicity.

Similarly, combining PTX (100 µg mL^{-1}) with Andrographolide (100 µg mL^{-1} and 200 µg mL^{-1}) reduced cell viability to 9.85 % and 9.25 %, respectively. The minimal difference between the two concentrations supports the notion that Andrographolide's effect is not due to its own cytotoxicity but rather to P-gp inhibitory activity, which helps overcome MDR and enhances PTX efficacy.

One-way analysis of variance (ANOVA) was used to assess the results statistically. (GraphPad Prism, v8.0.1), comparing the means of each treatment group to the PTX-only group (Figure 9). All groups showed statistically significant differences at $p < 0.0001$ with a high R^2 value (0.9265) and an F-value (31.49), reflecting substantial variation between groups. These statistical findings further support the reliability and significance of the observed therapeutic effects.

The present research findings support the use of Andrographolide as an effective P-gp inhibitor, comparable to the reference EPI (Verapamil), enhancing PTX cell internalization and cytotoxicity through the reversal of MDR. Moreover, unlike Verapamil, Andrographolide does not exhibit L-type calcium channel-blocking activity, thereby reducing the risk of cardiovascular side effects.[57,58] Additionally, Andrographolide exhibits anti-inflammatory, antioxidant, and anticancer properties.[59,60] These promising features support further developing Andrographolide as a natural, multifunctional, and safer chemo-sensitizer in cancer therapy.[61,62]

4 Conclusions

The present study identified Andrographolide as a promising natural P-gp inhibitor through combined *in silico* and *in vitro* evaluation, including cell line studies. Among 37 phytochemicals tested, Andrographolide showed a strong

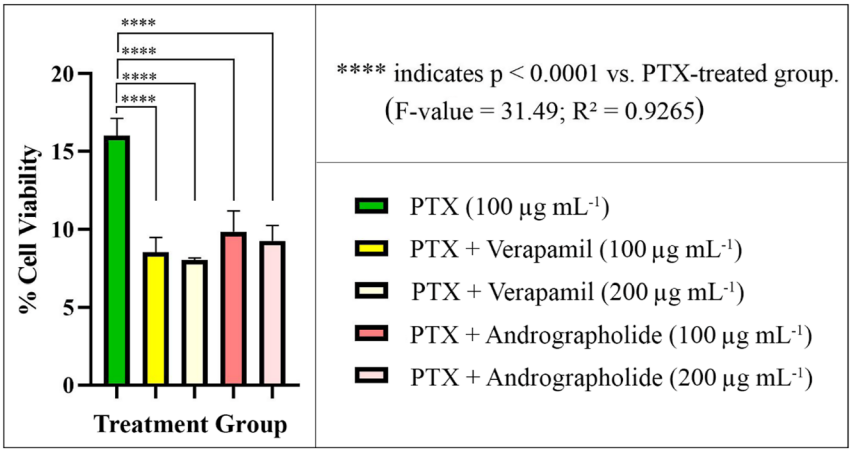

Figure 9: Comparison of cell viability across different treatment groups.

binding affinity, as well as stable and favourable interactions with the P-gp protein (PDB ID: 6FN1). Molecular docking, MM-GBSA, and superimposition analysis confirmed a strong binding affinity of the compound to the P-gp protein, comparable to that of Verapamil (a reference P-gp inhibitor). Furthermore, the *in vitro* MTT assay results indicate that Andrographolide enhanced PTX cytotoxicity in P-gp-expressing cells, comparable to Verapamil. Cell viability results showed exhibited no inherent cytotoxicity of Andrographolide at effective concentrations, further supporting its role in reversing MDR, and not in direct cell killing. The study findings support the promising use of Andrographolide in enhancing the intracellular accumulation of other P-gp substrate drugs. Therefore, co-administration of phytoconstituents like Andrographolide as a natural MDR modulator may reduce drug resistance and improve chemotherapy outcomes. However, further preclinical or pharmacokinetic studies are needed for clinical translation.

Acknowledgments: The authors are grateful to the online database such as RCSB PDB and PubChem (National Library of Medicine, NCBI) that were instrumental in collecting the data for in silico studies conducted in present work.

Research ethics: Not applicable.

Informed consent: Not applicable.

Author contributions: All authors have accepted responsibility for the entire content of this manuscript and approved its submission. Vijeth N. Bhat: Investigation; Methodology; Software; Data curation; Roles/Writing - original draft. Vinod L. Gaikwad: Conceptualization; Methodology; Formal analysis; Project administration; Resources; Software; Supervision; Validation; Writing - review & editing.

Use of Large Language Models, AI and Machine Learning Tools: None declared.

Conflict of interest: The authors state no conflict of interest.

Research funding: None declared.

Data availability: The authors confirm that the data supporting the findings of this study are available within the article.

References

1. Norouzi, M.; Hardy, P. Clinical Applications of Nanomedicines in Lung Cancer Treatment. *Acta Biomater*. **2021**, *121*, 134–142. https://doi.org/10.1016/j.actbio.2020.12.009.
2. Bukowski, K.; Kciuk, M.; Kontek, R. Mechanisms of Multidrug Resistance in Cancer Chemotherapy. *Int. J. Mol. Sci*. **2020**, *21* (9), 3233. https://doi.org/10.3390/ijms21093233.
3. Burchenal, J. H.; Robinson, E.; Johnston, S. F.; Kushida, M. N. The Induction of Resistance to 4-Amino-N ^{10}-Methyl-Pteroylglutamic Acid in a Strain of Transmitted Mouse Leukemia. *Science (1979)* **1950**, *111* (2875), 116–117. https://doi.org/10.1126/science.111.2875.116.
4. Marques, S. M.; Šupolíková, L.; Molčanová, L.; Šmejkal, K.; Bednar, D.; Slaninová, I. Screening of Natural Compounds as P-Glycoprotein Inhibitors against Multidrug Resistance. *Biomedicines* **2021**, *9* (4), 357. https://doi.org/10.3390/biomedicines9040357.
5. Gaikwad, V. L.; Bhatia, M. S. Polymers Influencing Transportability Profile of Drug. *Saudi Pharm. J.* **2013**, *21* (4), 327–335. https://doi.org/10.1016/j.jsps.2012.10.003.
6. Chen, C.; Chin, J. E.; Ueda, K.; Clark, D. P.; Pastan, I.; Gottesman, M. M.; Roninson, I. B. Internal Duplication and Homology with Bacterial Transport Proteins in the Mdr1 (P-Glycoprotein) Gene from Multidrug-Resistant Human Cells. *Cell* **1986**, *47* (3), 381–389. https://doi.org/10.1016/0092-8674(86)90595-7.
7. Ganesan, M.; Kanimozhi, G.; Pradhapsingh, B.; Khan, H. A.; Alhomida, A. S.; Ekhzaimy, A.; Brindha, G.; Prasad, N. R. Phytochemicals Reverse P-Glycoprotein Mediated Multidrug Resistance via Signal Transduction Pathways. *Biomed. Pharmacother.* **2021**, *139*, 111632. https://doi.org/10.1016/j.biopha.2021.111632.
8. Najar, I. A.; Sachin, B. S.; Sharma, S. C.; Satti, N. K.; Suri, K. A.; Johri, R. K. Modulation of P-Glycoprotein ATPase Activity by Some Phytoconstituents. *Phytother Res.* **2010**, *24* (3), 454–458. https://doi.org/10.1002/ptr.2951.
9. Ahmed Juvale, I. I.; Abdul Hamid, A. A.; Abd Halim, K. B.; Che, H.; P-Glycoprotein, A. T. New Insights into Structure, Physiological Function, Regulation and Alterations in Disease. *Heliyon* **2022**, *8* (6), e09777. https://doi.org/10.1016/j.heliyon.2022.e09777.
10. Kulkarni, A. S.; Kasabe, A. J.; Bhatia, M. S.; Bhatia, N. M.; Gaikwad, V. L. Quantitative Structure–Property Relationship Approach in Formulation Development: An Overview. *AAPS PharmSciTech* **2019**, *20* (7), 268. https://doi.org/10.1208/s12249-019-1480-2.
11. Gaikwad, V. L.; Bhatia, M. S.; Singhvi, I. Statistical Significance of Polymeric Physicochemical Properties in the Development of Formulations Containing a Drug from Neutral Class. *Arab. J. Chem.* **2016**, *9*, S1915–S1927. https://doi.org/10.1016/j.arabjc.2015.06.022.
12. Bhatia, N. M.; Gaikwad, V. L.; Mane, R. V.; Dhavale, R. P.; Bhatia, M. S. Quantitative Structure–Property Relationship Modeling for the Prediction of Hydrophilic Drug Entrapment in Liposomes for Lung Targeted Delivery. *New J. Chem.* **2018**, *42* (6), 4384–4393. https://doi.org/10.1039/C7NJ05190E.
13. Kasabe, A. J.; Kulkarni, A. S.; Gaikwad, V. L. QSPR Modeling of Biopharmaceutical Properties of Hydroxypropyl Methylcellulose (Cellulose Ethers) Tablets Based on its Degree of Polymerization. *AAPS PharmSciTech* **2019**, *20* (8), 308. https://doi.org/10.1208/s12249-019-1514-9.
14. Patil, R. S.; Kulkarni, S. B.; Gaikwad, V. L. Artificial Intelligence in Pharmaceutical Regulatory Affairs. *Drug Discov. Today* **2023**, *28* (9), 103700. https://doi.org/10.1016/j.drudis.2023.103700.
15. Bhat, V. N.; Bharati, S.; Bothiraja, C.; Sangshetti, J.; Gaikwad, V. A Review on Intervention of AI in Pharmaceutical Sector: Revolutionizing Drug Discovery and Manufacturing. *Intell. Pharm.* **2025**, *3* (5), 342–349. https://doi.org/10.1016/j.ipha.2025.04.001.
16. Mussard, E.; Cesaro, A.; Lespessailles, E.; Legrain, B.; Berteina-Raboin, S.; Toumi, H. Andrographolide, A Natural Antioxidant: An Update. *Antioxidants* **2019**, *8* (12), 571. https://doi.org/10.3390/antiox8120571.
17. Ketterman, A. J.; Wongtrakul, J.; Saisawang, C. Phytochemical Andrographolide Modulates NF-KB and JNK in Human Neuroblastoma

SH-SY5Y Cells, a Cell Model for Parkinson's Disease. *Heliyon* **2020**, *6* (6), e04121. https://doi.org/10.1016/j.heliyon.2020.e04121.
18. Pasha, A.; Ravinder, D.; Pawar, S. C. Andrographolide Mitigates Cisplatin Resistance by Inhibiting SPP1 Regulated NF-kB/INOS/COX-2 and PI3K/AKT Pathway in Cisplatin Resistant Cervical Carcinoma Cells. *Drug Dev. Res*. **2025**, *86* (1), e70052. https://doi.org/10.1002/ddr.70052.
19. Chatterjee, S.; Jain, S.; Jangid, R.; Sharma, M. K. Cytochrome P450 and P-gp mediated herb–drug interactions of some common indian herbs. In *Studies in Natural Products Chemistry*; Atta-ur-Rahman, Ed.; Elsevier: Amsterdam, Netherlands, 2022, Vol. 72, pp 225–258. https://doi.org/10.1016/B978-0-12-823944-5.00005-3.
20. Qiu, F.; Hou, X.-L.; Takahashi, K.; Chen, L.-X.; Azuma, J.; Kang, N. Andrographolide Inhibits the Expression and Metabolic Activity of Cytochrome P450 3A4 in the Modified Caco-2 Cells. *J. Ethnopharmacol.* **2012**, *141* (2), 709–713. https://doi.org/10.1016/j.jep.2011.09.002.
21. Alam, A.; Küng, R.; Kowal, J.; McLeod, R. A.; Tremp, N.; Broude, E. V.; Roninson, I. B.; Stahlberg, H.; Locher, K. P. Structure of a Zosuquidar and UIC2-Bound Human-Mouse Chimeric ABCB1. *Proc. Natl. Acad. Sci.* **2018**, *115* (9), E1973–E1982. https://doi.org/10.1073/pnas.1717044115.
22. Milroy, R. A Randomised Clinical Study of Verapamil in Addition to Combination Chemotherapy in Small Cell Lung Cancer. *Br. J. Cancer* **1993**, *68* (4), 813–818. https://doi.org/10.1038/bjc.1993.433.
23. Lusvarghi, S.; Robey, R. W.; Gottesman, M. M.; Ambudkar, S. V. Multidrug Transporters: Recent Insights from Cryo-Electron Microscopy-Derived Atomic Structures and Animal Models. *F1000Res.* **2020**, *9*, 17. https://doi.org/10.12688/f1000research.21295.1.
24. Schrödinger, Inc Protein Preparation Workflow. https://www.schrodinger.com/life-science/learn/white-papers/protein-preparation-workflow/ (accessed 08 18, 2025).
25. schrodinger, Inc LigPrep. https://www.schrodinger.com/platform/products/ligprep/ (accessed 08 18, 2025).
26. Sahayarayan, J. J.; Rajan, K. S.; Vidhyavathi, R.; Nachiappan, M.; Prabhu, D.; Alfarraj, S.; Arokiyaraj, S.; Daniel, A. N. In-Silico Protein-Ligand Docking Studies against the Estrogen Protein of Breast Cancer Using Pharmacophore Based Virtual Screening Approaches. *Saudi J. Biol. Sci.* **2021**, *28* (1), 400–407. https://doi.org/10.1016/j.sjbs.2020.10.023.
27. Madhavi Sastry, G.; Adzhigirey, M.; Day, T.; Annabhimoju, R.; Sherman, W. Protein and Ligand Preparation: Parameters, Protocols, and Influence on Virtual Screening Enrichments. *J. Comput. Aided Mol. Des.* **2013**, *27* (3), 221–234. https://doi.org/10.1007/s10822-013-9644-8.
28. Wang, E.; Sun, H.; Wang, J.; Wang, Z.; Liu, H.; Zhang, J. Z. H.; Hou, T. End-Point Binding Free Energy Calculation with MM/PBSA and MM/GBSA: Strategies and Applications in Drug Design. *Chem. Rev*. **2019**, *119* (16), 9478–9508. https://doi.org/10.1021/acs.chemrev.9b00055.
29. Sobh, E. A.; Dahab, M. A.; Elkaeed, E. B.; Alsfouk, B. A.; Ibrahim, I. M.; Metwaly, A. M.; Eissa, I. H. A Novel Thieno[2,3- *D*]Pyrimidine Derivative Inhibiting Vascular Endothelial Growth Factor Receptor-2: a Story of Computer-Aided Drug Discovery. *Drug Dev. Res*. **2023**, *84* (6), 1247–1265. https://doi.org/10.1002/ddr.22083.
30. Lindert, S.; Durrant, J. D.; McCammon, J. A. LigMerge: a Fast Algorithm to Generate Models of Novel Potential Ligands from Sets of Known Binders. *Chem. Biol. Drug Des*. **2012**, *80* (3), 358–365. https://doi.org/10.1111/j.1747-0285.2012.01414.x.
31. Pattar, S. V.; Adhoni, S. A.; Kamanavalli, C. M.; Kumbar, S. S. In Silico Molecular Docking Studies and MM/GBSA Analysis of Coumarin-Carbonodithioate Hybrid Derivatives Divulge the Anticancer Potential against Breast Cancer. *Beni-Suef Univ. J. Basic Appl. Sci.* **2020**, *9* (1), 36. https://doi.org/10.1186/s43088-020-00059-7.
32. Pandey, R.; Choudhary, K.; Prasad, S. R.; Kumar, P.; Bisht, P.; Aishwarya, D.; Nikhil, P.; Kumar, S.; Peraman, R.; Kumar, N. Mechanistic and Metabolic Exploration of Neohesperidin against Lung Cancer Cell Lines through ROS-Mediated Mitochondrial Apoptosis: an in-Silico and in-Vitro Approach. *Toxicol. Appl. Pharmacol*. **2025**, *499*, 117350. https://doi.org/10.1016/j.taap.2025.117350.
33. Natoli, M.; Leoni, B. D.; D'Agnano, I.; Zucco, F.; Felsani, A. Good Caco-2 Cell Culture Practices. *Toxicol. in Vitro* **2012**, *26* (8), 1243–1246. https://doi.org/10.1016/j.tiv.2012.03.009.
34. Bouquet, W.; Boterberg, T.; Ceelen, W.; Pattyn, P.; Peeters, M.; Bracke, M.; Remon, J. P.; Vervaet, C. In Vitro Cytotoxicity of Paclitaxel/β-Cyclodextrin Complexes for HIPEC. *Int. J. Pharm*. **2009**, *367* (1–2), 148–154. https://doi.org/10.1016/j.ijpharm.2008.09.035.
35. Miao, Q.; Wang, Z.; Zhang, Y.; Miao, P.; Zhao, Y.; Zhang, Y.; Ma, S. *In Vitro* Potential Modulation of Baicalin and Baicalein on P-Glycoprotein Activity and Expression in Caco-2 Cells and Rat Gut Sacs. *Pharm. Biol.* **2016**, *54* (9), 1548–1556. https://doi.org/10.3109/13880209.2015.1107744.
36. Martinec, O.; Biel, C.; de Graaf, I. A. M.; Huliciak, M.; de Jong, K. P.; Staud, F.; Cecka, F.; Olinga, P.; Vokral, I.; Cerveny, L. Rifampicin Induces Gene, Protein, and Activity of P-Glycoprotein (ABCB1) in Human Precision-Cut Intestinal Slices. *Front. Pharmacol* **2021**, *12*, e70052. https://doi.org/10.3389/fphar.2021.684156.
37. Dewanjee, S.; Dua, T.; Bhattacharjee, N.; Das, A.; Gangopadhyay, M.; Khanra, R.; Joardar, S.; Riaz, M.; Feo, V.; Zia-Ul-Haq, M. Natural Products as Alternative Choices for P-Glycoprotein (P-Gp) Inhibition. *Molecules* **2017**, *22* (6), 871. https://doi.org/10.3390/molecules22060871.
38. Lai, J.-I.; Tseng, Y.-J.; Chen, M.-H.; Huang, C.-Y. F.; Chang, P. M.-H. Clinical Perspective of FDA Approved Drugs with P-Glycoprotein Inhibition Activities for Potential Cancer Therapeutics. *Front. Oncol.* **2020**, *10*, 561936. https://doi.org/10.3389/fonc.2020.561936.
39. Fukunishi, Y.; Yamashita, Y.; Mashimo, T.; Nakamura, H. Prediction of Protein−Compound Binding Energies from Known Activity Data: Docking-Score-Based Method and its Applications. *Mol. Inform.* **2018**, *37* (6–7). https://doi.org/10.1002/minf.201700120.
40. Arshad, N.; Abbas, N.; Perveen, F.; Mirza, B.; Almuhaini, A. M.; Alkahtani, S. Molecular Docking Analysis and Spectroscopic Investigations of Zinc(II), Nickel(II) N-Phthaloyl-β-Alanine Complexes for DNA Binding: Evaluation of Antibacterial and Antitumor Activities. *J. Saudi Chem. Soc.* **2021**, *25* (9), 101323. https://doi.org/10.1016/j.jscs.2021.101323.
41. Schrödinger. Docking and Scoring. https://www.schrodinger.com/life-science/learn/white-papers/docking-and-scoring/ (accessed 2025-12-27).
42. Glide Docking, Autodock, Binding Free Energy and Drug-Likeness Studies for Prediction of Potential Inhibitors of Cyclin-Dependent Kinase 14 Protein in Wnt Signaling Pathway. Biointerface Res. Appl. Chem. **2021**, *12* (2), 2473–2488. https://doi.org/10.33263/BRIAC122.24732488.
43. Du, X.; Li, Y.; Xia, Y.-L.; Ai, S.-M.; Liang, J.; Sang, P.; Ji, X.-L.; Liu, S.-Q. Insights into Protein–Ligand Interactions: Mechanisms, Models, and Methods. *Int. J. Mol. Sci.* **2016**, *17* (2), 144. https://doi.org/10.3390/ijms17020144.
44. Mulakala, C.; Viswanadhan, V. N. Could MM-GBSA be Accurate Enough for Calculation of Absolute Protein/Ligand Binding Free Energies? *J. Mol. Graph. Model.* **2013**, *46*, 41–51. https://doi.org/10.1016/j.jmgm.2013.09.005.
45. Sumita, A.; Shoba, G.; Thamarai Selvan, R.; Anju, K.; Balakumaran, M. D.; Kumaran, R. Photophysical and Molecular Docking Studies of Photoinduced Electron Transfer (PET) and Non-PET Based Fluorophores of Acridinedione Derivatives with a Glycoprotein: Ovalbumin. *Results Chem.* **2021**, *3*, 100187. https://doi.org/10.1016/j.rechem.2021.100187.
46. Malau, N. D.; Azzahra, S. F. Molecular Docking Studies of Potential Quercetin 3,4'-Dimethyl Ether 7-Alpha-LArabinofuranosyl-(1-6)-

Glucoside as Inhibitor Antimalaria. *J. Phys. Conf. Ser.* **2020**, *1428* (1), 012057. https://doi.org/10.1088/1742-6596/1428/1/012057.
47. Shamsian, S.; Sokouti, B.; Dastmalchi, S. Benchmarking Different Docking Protocols for Predicting the Binding Poses of Ligands Complexed with Cyclooxygenase Enzymes and Screening Chemical Libraries. *BioImpacts* **2023**, *14*, 29955. https://doi.org/10.34172/bi.2023.29955.
48. Genheden, S.; Kuhn, O.; Mikulskis, P.; Hoffmann, D.; Ryde, U. The Normal-Mode Entropy in the MM/GBSA Method: Effect of System Truncation, Buffer Region, and Dielectric Constant. *J. Chem. Inf. Model*. **2012**, *52* (8), 2079–2088. https://doi.org/10.1021/ci3001919.
49. Syed, S. B.; Arya, H.; Fu, I.-H.; Yeh, T.-K.; Periyasamy, L.; Hsieh, H.-P.; Coumar, M. S. Targeting P-Glycoprotein: Investigation of Piperine Analogs for Overcoming Drug Resistance in Cancer. *Sci. Rep*. **2017**, *7* (1), 7972. https://doi.org/10.1038/s41598-017-08062-2.
50. Fu, Y.; Zhao, J.; Chen, Z. Insights into the Molecular Mechanisms of Protein-Ligand Interactions by Molecular Docking and Molecular Dynamics Simulation: A Case of Oligopeptide Binding Protein. *Comput. Math. Methods Med.* **2018**, *2018*, 1–12. https://doi.org/10.1155/2018/3502514.
51. Mansour, F. R.; Elhosary, N.; Elagamy, S. H.; Barseem, A.; Kamal, A. H. Multi Spectroscopic Investigations with Molecular Docking and Molecular Dynamics Simulation of the Binding Mechanism of Molnupiravir to Bovine Serum Albumin. *BMC Chem.* **2025**, *19* (1), 286. https://doi.org/10.1186/s13065-025-01645-5.
52. Lobanov, M. Y.; Bogatyreva, N. S.; Galzitskaya, O. V. Radius of Gyration as an Indicator of Protein Structure Compactness. *Mol. Biol.* **2008**, *42* (4), 623–628. https://doi.org/10.1134/S0026893308040195.
53. Bogatyreva, N. S.; Ivankov, D. N. The Relationship between the Solvent-Accessible Surface Area of a Protein and the Number of Native Contacts in its Structure. *Mol. Biol.* **2008**, *42* (6), 932–938. https://doi.org/10.1134/S0026893308060150.
54. Vishvakarma, V. K.; Singh, M. B.; Jain, P.; Kumari, K.; Singh, P. Hunting the Main Protease of SARS-CoV-2 by Plitidepsin: Molecular Docking and Temperature-Dependent Molecular Dynamics Simulations. *Amino Acids* **2022**, *54* (2), 205–213. https://doi.org/10.1007/s00726-021-03098-1.
55. Jorgensen, C.; Ulmschneider, M. B.; Searson, P. C. Modeling Substrate Entry into the P-Glycoprotein Efflux Pump at the Blood–Brain Barrier. *J. Med. Chem*. **2023**, *66* (24), 16615–16627. https://doi.org/10.1021/acs.jmedchem.3c01069.
56. Pires, M. M.; Emmert, D.; Hrycyna, C. A.; Chmielewski, J. Inhibition of P-Glycoprotein-Mediated Paclitaxel Resistance by Reversibly Linked Quinine Homodimers. *Mol. Pharmacol*. **2009**, *75* (1), 92–100. https://doi.org/10.1124/mol.108.050492.
57. Chen, N. X.; Kircelli, F.; O'Neill, K. D.; Chen, X.; Moe, S. M. Verapamil Inhibits Calcification and Matrix Vesicle Activity of Bovine Vascular Smooth Muscle Cells. *Kidney Int*. **2010**, *77* (5), 436–442. https://doi.org/10.1038/ki.2009.481.
58. Shen, Y.; Chen, C.; Chiou, W. Andrographolide Prevents Oxygen Radical Production by Human Neutrophils: Possible Mechanism(s) Involved in its Anti-Inflammatory Effect. *Br. J. Pharmacol*. **2002**, *135* (2), 399–406. https://doi.org/10.1038/sj.bjp.0704493.
59. Ribeiro, J. R. L.; Szemerédi, N.; Gonçalves, B. M. F.; Spengler, G.; Afonso, C. A. M.; Ferreira, M.-J. U. Nitrogen-Containing Andrographolide Derivatives with Multidrug Resistance Reversal Effects in Cancer Cells. *RSC Med. Chem*. **2024**, *15* (4), 1348–1361. https://doi.org/10.1039/D3MD00711A.
60. Luo, S.; Li, H.; Liu, J.; Xie, X.; Wan, Z.; Wang, Y.; Zhao, Z.; Wu, X.; Li, X.; Yang, M.; Li, X. Andrographolide Ameliorates Oxidative Stress, Inflammation and Histological Outcome in Complete Freund's Adjuvant-Induced Arthritis. *Chem. Biol. Interact.* **2020**, *319*, 108984. https://doi.org/10.1016/j.cbi.2020.108984.
61. Nguyen, T.-T.-L.; Duong, V.-A.; Maeng, H.-J. Pharmaceutical Formulations with P-Glycoprotein Inhibitory Effect as Promising Approaches for Enhancing Oral Drug Absorption and Bioavailability. *Pharmaceutics* **2021**, *13* (7), 1103. https://doi.org/10.3390/pharmaceutics13071103.
62. Nanayakkara, A. K.; Follit, C. A.; Chen, G.; Williams, N. S.; Vogel, P. D.; Wise, J. G. Targeted Inhibitors of P-Glycoprotein Increase Chemotherapeutic-Induced Mortality of Multidrug Resistant Tumor Cells. *Sci. Rep*. **2018**, *8* (1), 967. https://doi.org/10.1038/s41598-018-19325-x.

Bionotes

Vijeth N. Bhat
Vijeth N. Bhat is a Post-Graduate Research Scholar (C/O Dr. Gaikwad) in the Department of Pharmaceutics at NIPER Hajipur (Bihar, India), with research interests in herbal medicines and nanoparticles in cancer-targeted drug delivery technologies.

Vinod L. Gaikwad
Vinod L. Gaikwad is an Assistant Professor in the Department of Pharmaceutics at NIPER Hajipur (Bihar, India). His research interests include formulation development and drug delivery integrated with AI and computational approaches.